Chemical Science

ROYAL SOCIETY OF CHEMISTRY

EDGE ARTICLE

View Article Online
View Journal | View Issue

Cite this: *Chem. Sci.*, 2025, **16**, 8897

All publication charges for this article have been paid for by the Royal Society of Chemistry

Cooperative promotion of electroreduction of CO to *n*-propanol by *CO enrichment and proton regulation†

Rongxing Qiu,[a] Linxiao Cui,[a] Li Peng,*[a] Olga A. Syzgantseva,[b] Jiaran Li,[a] Nan Fang,[a] Maria A. Syzgantseva,[c] Yuan Jiang,[a] Jie Zhang,[d] Bingxing Zhang,[e] Lingzhi Ding,[a] Yangyang Dong,[a] Tianwei Xue,[a] Cheng Li,[a] Jin-Chao Dong,[a] Jinyu Ye,[a] Isil Akpinar,[f] Shuliang Yang,*[a] Jun Li,*[a] Jianling Zhang,[g] Jian-Feng Li[a] and Buxing Han*[g]

The CO_2/CO electroreduction reaction (CO_2RR/CORR) to liquid products presents an enticing pathway to store intermittent renewable electricity. However, the selectivity for desirable high-value C_3 products, such as *n*-propanol, remains unsatisfactory in the CO_2RR/CORR. Here, we report that *CO enrichment and proton regulation cooperatively enhance C_1–C_2 coupling by increasing CO pressure and utilizing proton sponge modification, promoting the production of *n*-propanol over a Cu^0/Cu^+ nanosheet catalyst in the CORR. We obtain an impressive faradaic efficiency (FE) of 44.0% ± 2.3% for *n*-propanol at a low potential of −0.44 V *vs.* reversible hydrogen electrode (RHE) under 3 bar CO. Experimental results demonstrated that *H intermediates could be regulated by proton sponge modification. *In situ* characterization combined with density functional theory (DFT) calculations validate that Cu^+ species exist stably in proton sponge-modified Cu-based catalysts along with appropriate *CO coverage. This design facilitates the potential-determining C_1–C_1 and C_1–C_2 coupling steps and contributes to the *n*-propanol production.

Received 13th January 2025
Accepted 10th April 2025

DOI: 10.1039/d5sc00274e

rsc.li/chemical-science

Introduction

Electrochemical CO_2 reduction reaction (CO_2RR) to high value-added chemical feedstocks and fuels is a promising route for the storage of renewable electricity.[1] Presently, much progress has been made in the CO_2RR, however, the major products with satisfying performance reported are limited to C_1 (CO,[2,3] CH_4,[4–6] $HCOO^-$,[7] and CH_3OH[8,9]) and C_2 (C_2H_4,[10–12] C_2H_5OH,[13–15] and CH_3COOH[16]) products. C_3 products such as *n*-propanol, a high value-added and high energy-density chemical, have been produced with low FE in previous reports in the CO_2RR.[17–19] Besides, electrolytes with alkaline or neutral pH are typically employed in the CO_2RR, which leads to undesired carbonate formation easily, causing energy/carbon losses and performance degradation.[20] Given the conspicuous progress of the highly efficient CO_2RR to CO,[21] the *n*-propanol chemical produced by the electrochemical reduction reaction of CO (CORR) following the high-performance CO_2 reduction to CO, could efficiently alleviate these problems.[22,23]

Cu-based materials have been reported to be efficient electrocatalysts for producing C_3 products such as *n*-propanol. Recently, various strategies have been adopted to enhance the FE of *n*-propanol with Cu-based catalysts, including the engineering of the oxidation state of Cu atoms,[24] morphological tuning,[25–27] Cu-based multimetallic materials,[28–31] grain boundary control,[32] selective formation of the desired facets,[33] *etc*. However, these catalysts still suffer from several challenges, such as limited selectivity in producing *n*-propanol (Table S1†). Thus, developing new approaches to enhance *n*-propanol selectivity in the CORR is still highly challenging and desirable.

As demonstrated in the published reports, high *CO coverage is beneficial for the formation of C_{2+} alcohol products

[a]College of Chemistry and Chemical Engineering, College of Energy, Xiamen University, Xiamen, 361005, Fujian, P. R. China. E-mail: li.peng@xmu.edu.cn; ysl@xmu.edu.cn; junnyxm@xmu.edu.cn
[b]Lomonosov Moscow State University, Peoples' Friendship University of Russia, Russia/Department of Chemistry, Moscow, 119991, Russia
[c]Department of Physics, Mendeleev University of Chemical Technology, Moscow, 125047, Russia
[d]Institute of Chemical Sciences and Engineering, École Polytechnique Fédérale de Lausanne (EPFL), 1951 Sion, Switzerland
[e]School of Materials Science and Engineering, Zhejiang University, Hangzhou, 310058, Zhejiang, P.R. China
[f]Department of Chemistry and International Institute of Nanotechnology, Northwestern University, 2145 Sheridan Road, Evanston, IL 60208, USA
[g]Beijing National Laboratory for Molecular Sciences, CAS Key Laboratory of Colloid and Interface and Thermodynamics, CAS Research/Education Center for Excellence in Molecular Sciences, Institute of Chemistry, Chinese Academy of Sciences, Beijing, 100190, P.R. China. E-mail: hanbx@iccas.ac.cn

† Electronic supplementary information (ESI) available. See DOI: https://doi.org/10.1039/d5sc00274e

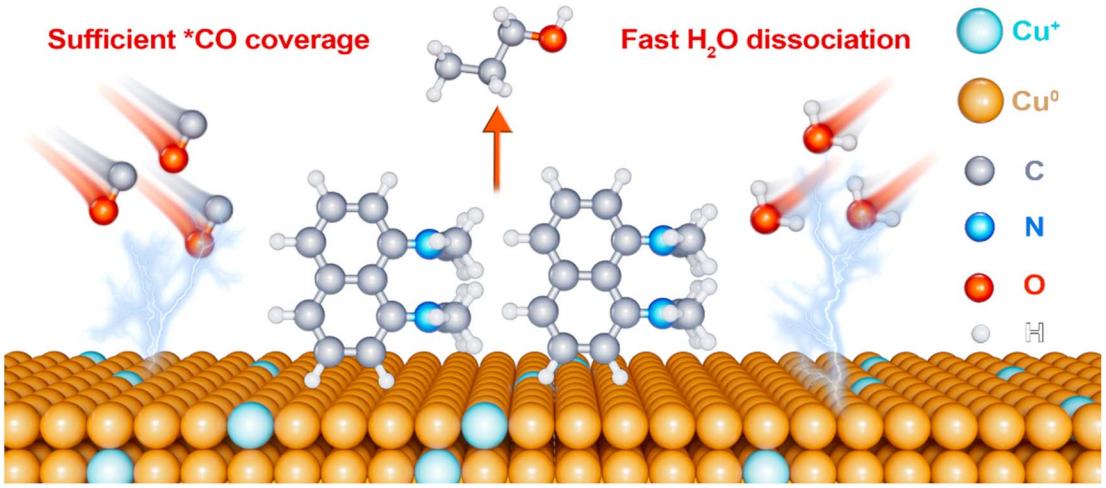

Scheme 1 Schematic illustration of CO electrolysis to *n*-propanol with proton sponge-modified Cu nanosheets as the catalyst under the assistance of CO pressures.

in CO_2/CO electrolysis.[34–37] Interestingly, our previous study of the CO_2RR showed that higher CO_2 pressure could enrich *CO coverage on the catalyst surface, which was beneficial to obtain the ethanol product rather than ethylene.[38] Considering that the pathway of the CORR to *n*-propanol is a multiple proton-coupled electron transfer process, sufficient supplies of *CO and *H intermediates are essential to produce *n*-propanol during the process. *CO coverage usually could be regulated by pressure variation, while *H intermediates could be modulated *via* a reductive concerted proton–electron transfer (CPET) mediator.[39,40] Proton sponge (1,8-bis(dimethylamino)naphthalene) shows exceptional proton affinity through bidentate-type coordination by the two dimethylamino groups located at the peri position of the naphthalene skeleton.[41–43] The general feature of all proton sponges is the presence of two basic nitrogen centers in the molecule, which have an orientation that allows the uptake of one proton to yield a stabilized intramolecular hydrogen bond (IMHB). The strength of the IMHB calculated for proton sponges is in the range of 16–21.5 kcal mol^{-1},[42,44] which is similar to that of the CPET mediator.

Herein, a cooperative strategy of applying pressure coupled with the use of a proton regulator (proton sponge, PS) for an efficient CORR to *n*-propanol was developed. A series of proton sponge-modified Cu nanosheet catalysts (denoted as Cu-NS-*x*% PS, $x = 0$, 10, 20, 30 and 50, where x is the mass percentage of proton sponge in the catalyst) were constructed. The CORR experiments were carried out under different CO pressures (0.5, 1, 2, 3 and 5 bar) with the as-prepared catalysts. Among these, the Cu-NS-20% PS catalyst for the CORR showed an *n*-propanol FE of 44.0% ± 2.3% at −0.44 V *vs.* RHE under 3 bar CO, representing ~1.4-fold improvement relative to the unmodified Cu-NS under the same CO pressure. Experimental results showed that *H intermediates could be adjusted *via* proton sponge modification. *In situ* attenuated-total-reflection surface-enhanced infrared absorption spectroscopy (*in situ* ATR-SEIRAS) indicated that sufficient *CO coverage could be provided by elevating CO pressure on the proton sponge modified Cu-NS catalyst for subsequent C–C coupling. *In situ* Raman spectra combined with DFT calculations further verified that Cu^+ species in the Cu-NS-20% PS catalyst was persistent during the CORR under 3 bar CO, which was also beneficial for stabilizing *CO, and facilitating both C_1–C_1 and C_1–C_2 coupling to produce the desired *n*-propanol. This work creatively demonstrated that the cooperative design of a proton regulator with appropriate CO pressure was highly capable of improving the electrosynthesis of *n*-propanol from CO and H_2O (Scheme 1).

Results and discussion

Catalyst preparation and characterization

Proton sponge-modified Cu nanosheet catalysts were prepared as displayed schematically in Fig. 1a. Firstly, CuO nanosheets (CuO-NS) were synthesized *via* a wet chemical method. Proton sponge-modified CuO nanosheets (CuO-NS-*x*% PS) were then obtained by the addition of 1,8-bis(dimethylamino)naphthalene (proton sponge) dissolved in isopropanol to CuO nanosheets. The representative scanning electron microscopy (SEM) (Fig. 1b) and transmission electron microscopy (TEM) images (Fig. 1c) displayed CuO-NS-20% PS with a nanosheet morphology, which was similar to that of CuO-NS and other CuO-NS-*x*% PS (Fig. S1 and S2†). The lattice distances of CuO-NS-20% PS and CuO-NS were observed clearly in the high-resolution transmission electron microscopy (HR-TEM) images (Fig. 1d, S3 and S4†), which corresponded to CuO (111) and CuO ($\bar{1}10$), respectively. Moreover, energy-dispersive X-ray spectroscopy (EDX) elemental mapping of CuO-NS-20% PS showed that the characteristic Cu, O and N elements were uniformly dispersed in CuO-NS-20% PS, indicating that the proton sponge was integrated very well (Fig. 1e). The successful proton sponge modification was further confirmed *via* Fourier-transform infrared spectroscopy (FT-IR), where representative absorption peaks from proton sponge were also well detected in

CuO-NS-20% PS (Fig. 1f). Powder X-ray diffraction patterns (PXRD) of CuO-NS-*x*% PS ($x = 10$, 20, 30 and 50) were consistent with those of CuO-NS (Fig. 1g). Raman spectra further demonstrated the characteristic peak of CuO at 276, 320, and 605 cm^{-1} for both CuO-NS and CuO-NS-20% PS (Fig. S5†).[45] These results revealed that the mild proton sponge-modification method would not affect the crystallinity of CuO. Additionally, X-ray photoelectron spectroscopy (XPS) was used to monitor the valence state of the catalysts. XPS spectrum of CuO-NS-20% PS revealed characteristic peaks of Cu^{2+} species at 954.3 eV (Cu $2p_{1/2}$) and 934.3 eV (Cu $2p_{3/2}$) (Fig. S6†). The N 1s XPS spectra further evidenced the successful proton sponge-modification (Fig. S7†). Moreover, the mole percentages of proton sponge in CuO-NS-*x*% PS were cross-checked by thermal gravimetric analysis (TGA), XPS, and SEM-EDX, indicating that the amount of modified PS could be easily regulated (Fig. S8 and Table S2†).

Cu-NS-*x*% PS catalysts ($x = 0$, 10, 20, 30 and 50) were obtained *via in situ* electroreduction of CuO-NS-*x*% PS upon four runs of linear sweep voltammetry (LSV) with a scan speed of 20 mV s^{-1} over a potential range from open-circuit potential (OCP) to −0.64 V *vs.* RHE. As observed in SEM and TEM images (Fig. 2a and b), Cu-NS-20% PS displayed a rougher surface with distinguishable nanoparticles on the nanosheet when compared with the precursor, CuO-NS-20% PS (Fig. 1b and c).[46] Due to the unavoidable oxidation during sample transfer in *ex situ* XRD, Cu_2O species were detected in both Cu-NS and Cu-NS-20% PS following electroreduction. The PXRD pattern of the Cu-NS-20% PS proved the formation of Cu^0 and Cu^+ species, and the major exposed planes were Cu_2O (111), Cu (111) and Cu (200) of face-centered cubic Cu (fcc-Cu), while Cu (111) was the most remarkable characteristic peak in the PXRD pattern of the pure Cu-NS sample (Fig. 2c). Cu LMM Auger spectra in Cu-NS-20% PS further confirmed the existence of Cu^+ species (Fig. S9†). To acquire more accurate surface features of the Cu-NS and proton sponge modified Cu-NS, we investigated the electrochemical adsorption of OH^- on the Cu-NS and Cu-NS-20% PS catalysts considering their facet-dependent OH^- adsorption behaviors. The cyclic voltammetry curves in

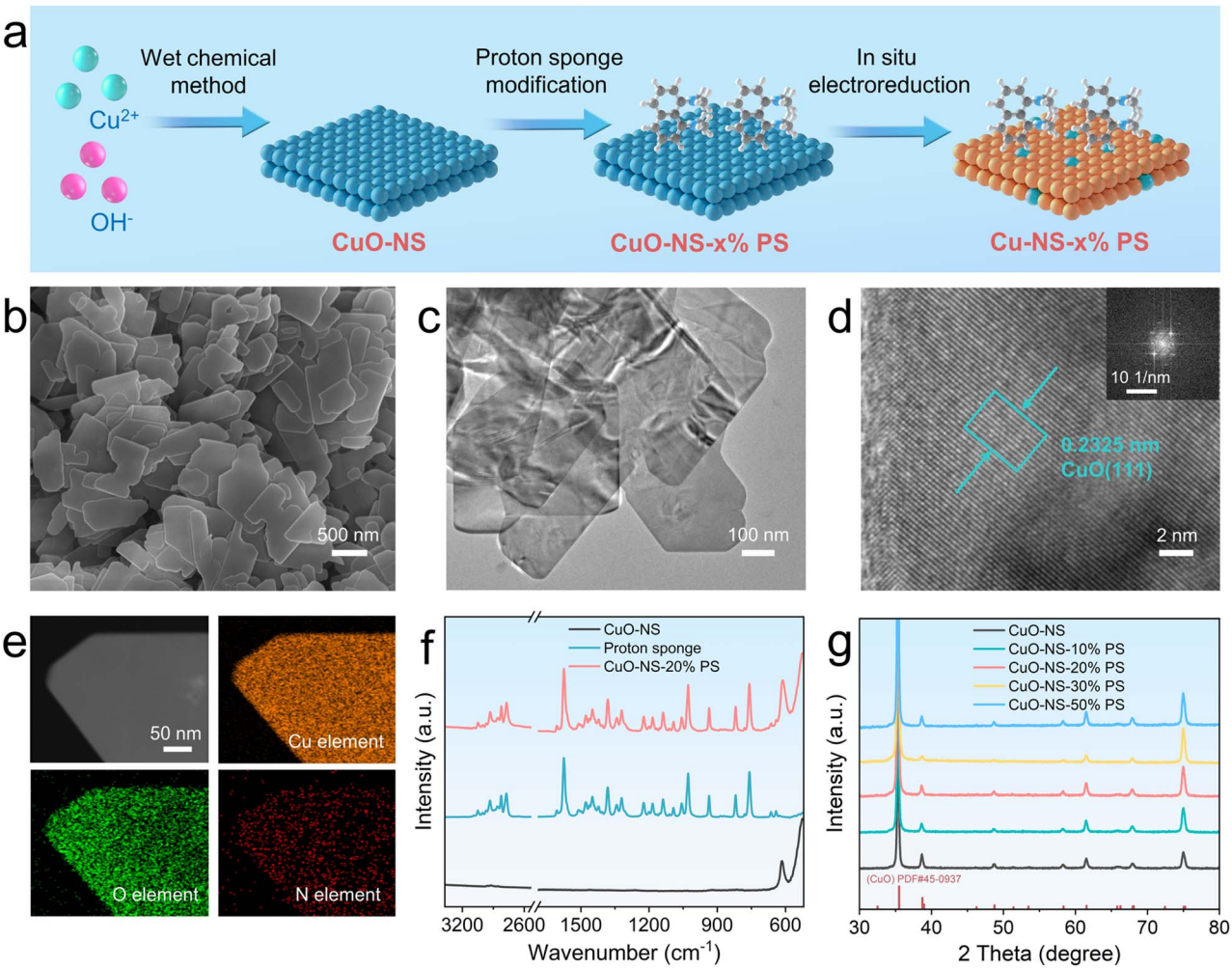

Fig. 1 Synthesis and characterization of CuO-NS-*x*% PS catalysts ($x = 0$, 10, 20, 30 and 50). (a) Schematic illustration of the synthetic procedure of Cu-NS-PS catalysts. (b) SEM, (c) TEM and (d) HRTEM images of CuO-NS-20% PS. (e) EDX elemental mappings of Cu, O and N in a single nanosheet of CuO-NS-20% PS. (f) FT-IR spectra of pure CuO-NS, proton sponge and CuO-NS-20% PS. (g) PXRD patterns of CuO-NS and CuO-NS-*x*% PS with different proton sponge loadings.

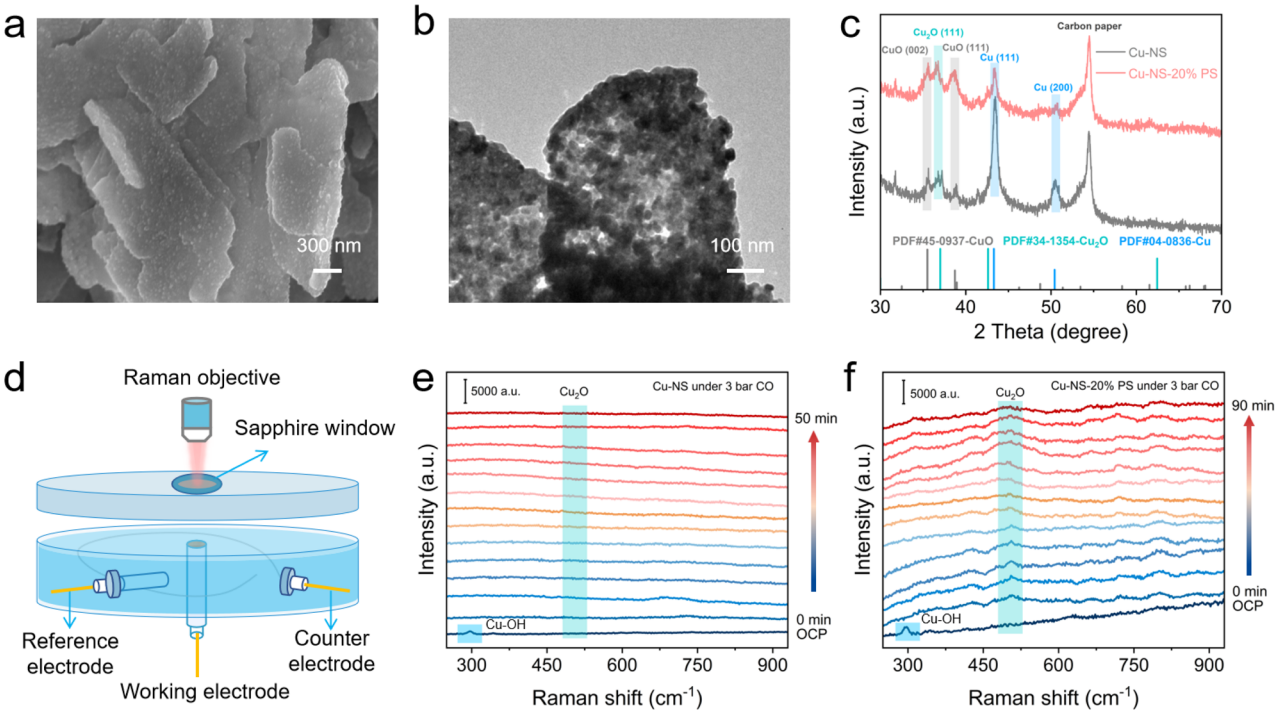

Fig. 2 Synthesis and characterization of Cu-NS-20% PS catalysts. (a) SEM and (b) TEM images of Cu-NS-20% PS. (c) PXRD patterns of Cu-NS and Cu-NS-20% PS. (d) Schematic illustration of the custom-made high-pressure *in situ* Raman cell setup for the CORR. (e) *In situ* Raman spectra of Cu-NS under 3 bar CO at −0.44 V *vs.* RHE for 50 min. (f) *In situ* Raman spectra of Cu-NS-20% PS under 3 bar CO at −0.44 V *vs.* RHE for 90 min. The electrode was pretreated *via in situ* electroreduction before recording the amperometric curve and *in situ* Raman spectra testing.

Fig. S10† showed OH^- adsorption peaks at around 0.40, 0.44 and 0.50 V *vs.* RHE for Cu-NS and Cu-NS-20% PS, corresponding to the OH^- adsorption on the Cu (100), Cu (110) and Cu (111) surfaces, respectively.[47–49] These results indicate that both Cu-NS and Cu-NS-20% PS are dominated by Cu {100}, {110} and {111} facets.

In situ Raman spectra were collected in a high-pressure *in situ* Raman cell setup (Fig. 2d), and Raman bands that appeared around 510 cm^{-1} belonging to Cu_2O[50–52] remained in the proton sponge-modified Cu-based catalysts (Cu-NS-20% PS and Cu-NS-50% PS) at −0.44 V *vs.* RHE during the *in situ* observation (Fig. 2f and S11†), while no Cu_2O was detected for the pure Cu-NS sample during the CORR process (Fig. 2e). These results validated that Cu^+ species existed stably in the proton sponge-modified Cu-based catalysts during the CORR process, which was obviously different from Cu-NS without proton sponge modification. In order to observe the detailed changes in the valence state of Cu species during the *in situ* electroreduction process, *in situ* PXRD and *in situ* Raman characterization were conducted. Results showed that the Cu-NS catalyst possessed both Cu^+ and Cu^0 before converting to Cu^0 completely (Fig. S12 and S13†).

CORR performance on proton sponge modified Cu-NS under different pressures

The electrocatalytic activity and selectivity for the CORR under different pressures were systematically evaluated in a custom-made pressurized cell with a two-compartment polytetrafluoroethylene (PTFE) lining separated by a proton exchange membrane (Fig. 3a and S14†). The CORR product distributions from Cu-NS and Cu-NS-20% PS under 1 bar and 3 bar CO are presented in Fig. 3b. As the CO pressure elevated from 1 bar to 3 bar, both Cu-NS and Cu-NS-20% PS exhibited an increase in $FE_{n\text{-propanol}}$ and $FE_{acetate}$, while the $FE_{C_2H_4}$ and FE_{H_2} decreased. Notably, compared with pure Cu-NS, the FE_{H_2} of proton sponge modified Cu-NS increased under ambient pressure, which was attributed to low *CO coverage and high *H intermediates caused by the proton sponge. While the FE_{H_2} of Cu-NS-20% PS under 3 bar CO was similar to that of Cu-NS under the same CO pressure, Cu-NS-20% PS exhibited higher $FE_{n\text{-propanol}}$ and lower $FE_{acetate}$. This was because the higher *CO coverage under 3 bar CO could match the higher *H intermediates to produce *n*-propanol rather than acetate. Overall, the $FE_{n\text{-propanol}}$ reached 44.0 ± 2.3% over Cu-NS-20% PS under 3 bar CO at −0.44 V *vs.* RHE, which was ~1.4-fold higher than that over the pure Cu-NS catalyst under the same CO pressure. Moreover, the total current density (j_{total}) and partial current density for *n*-propanol ($j_{n\text{-propanol}}$) of Cu-NS or Cu-NS-20% PS could be enhanced during the CORR when CO pressure elevated from 1 bar to 3 bar (Fig. 3c). The positive feedback further indicated that higher activity for producing *n*-propanol in the CORR could be achieved with the assistance of proton sponge under elevating CO pressure.

To explore the effects of CO pressure on CORR performance, CORR experiments with Cu-NS-20% PS at 0.5, 1, 2, 3 and 5 bar CO were further conducted (Fig. S19†). According to the

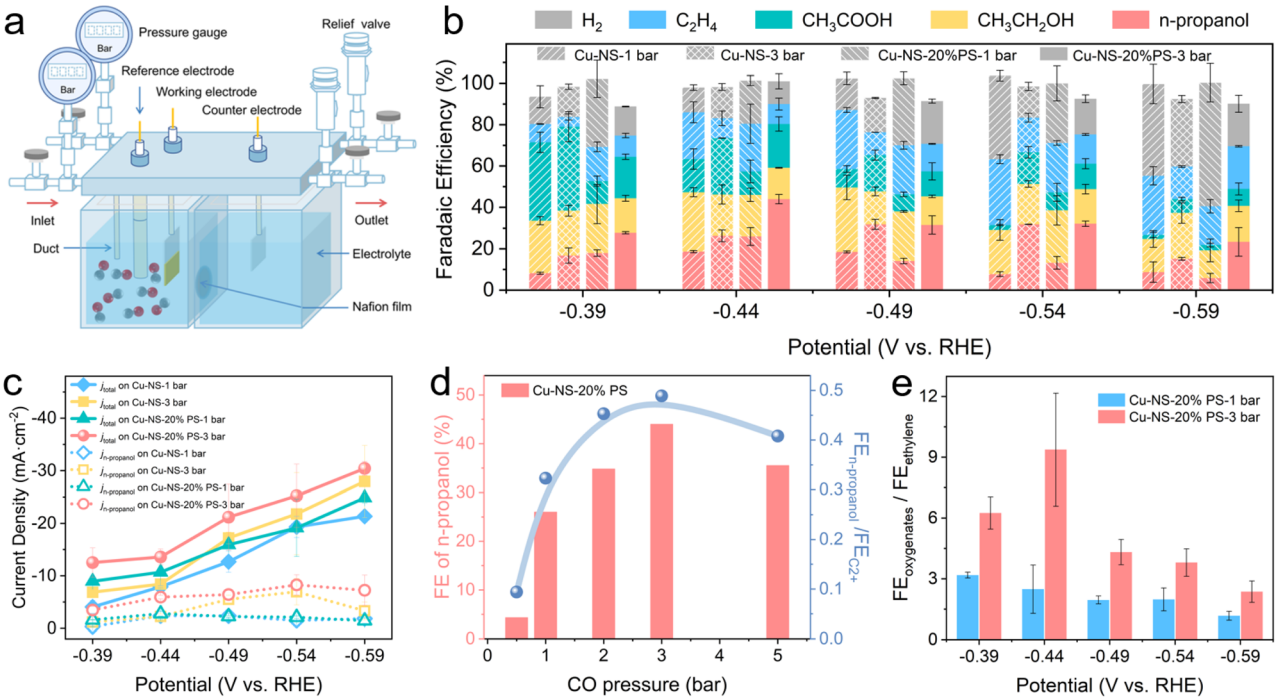

Fig. 3 Electrochemical CORR performances of Cu-NS and Cu-NS-20% PS under ambient and high CO pressures. (a) Schematic CORR setup under both ambient and high CO pressures. (b) CORR product distributions for Cu-NS and Cu-NS-20% PS under 1 bar and 3 bar CO, respectively. (c) The total current density (j_{total}) and partial current density for *n*-propanol ($j_{n\text{-propanol}}$) on Cu-NS-20% PS and Cu-NS catalysts under 1 bar, 3 bar CO *vs.* the cathodic potentials, respectively. (d) $FE_{n\text{-propanol}}$ and $FE_{n\text{-propanol}}/FE_{C_{2+}}$ ratios on Cu-NS-20% PS under different CO pressures (0.5, 1, 2, 3 and 5 bar CO). (e) $FE_{oxygenates}/FE_{ethylene}$ ratios on Cu-NS-20% PS under different CO pressures (1 bar *vs.* 3 bar CO). Error bars represent the standard deviation of three independent measurements.

experimental data, we built the correlations between $FE_{n\text{-propanol}}$ and CO pressures in the CORR with the Cu-NS-20% PS catalyst (Fig. 3d). $FE_{n\text{-propanol}}$ presented a volcanic trend with the CO pressures increased from 0.5 to 5 bar CO, in which $FE_{n\text{-propanol}}$ rose steeply with CO pressure increasing from 0.5 to 3 bar. $FE_{n\text{-propanol}}$ exhibited a drop when the CO pressure was further elevated to 5 bar, which could be attributed to excessive *CO coverage and insufficient *H intermediates required for the *n*-propanol production pathway. These results indicated that an appropriate *CO coverage was beneficial for C_1–C_1 coupling and C_1–C_2 coupling to produce *n*-propanol during the CORR process. We observed that the $FE_{oxygenates}/FE_{ethylene}$ ratio on Cu-NS-20% PS increased with the CO pressures elevated from 1 bar to 3 bar CO (Fig. 3e), and a similar trend appeared on Cu-NS (Fig. S20†). These results proved that oxygenated products could be enhanced accompanied by decreased ethylene by facilely increasing the CO pressure.[53,54] The CO pressure regulation could also remarkably affect the C_2 and C_3 selectivities in the CORR. In detail, with the CO pressure elevated, the FE of C_2H_4 and CH_3CH_2OH decreased, while the FE of CH_3COOH and *n*-propanol increased on the majority of nano Cu-based catalysts (Table S3†).

The role of proton sponge was then investigated. We conducted a series of CORR experiments on Cu-NS without proton sponge and Cu-NS-*x*% PS with different loadings of proton sponge ($x = 10$, 20, 30 and 50) under 3 bar CO pressure (Fig. 4a and S21†). Initially, with the increased amount of proton sponge in Cu-NS, the $FE_{n\text{-propanol}}$ was promoted efficiently, and reached the peak until Cu-NS combined with 20% of proton sponge, and then showed a downward trend. We also constructed the relationship between $FE_{n\text{-propanol}}/FE_{C_{2+}}$ ratio and the amount of proton sponge (Fig. 4a). The $FE_{n\text{-propanol}}/FE_{C_{2+}}$ ratio over Cu-NS-20% PS reached almost 0.5 under 3 bar CO, while the ratio was only 0.38 for Cu-NS under 3 bar CO, which evidenced that the *n*-propanol production was synergistically promoted by the proton sponge and elevating CO pressure. Interestingly, both $FE_{acetate}$ and the $FE_{acetate}/FE_{oxygenates}$ ratio dropped after being modified with 20% proton sponge on Cu-NS compared with the pure Cu-NS under the same CO pressure (Fig. 3b and 4b). Meanwhile, the proton sponge modified Cu-NS increased HER selectivity especially under ambient CO pressure (Fig. S22†). According to the above results, it can be concluded that acetate formation with the least proton requirement per carbon among the produced oxygenates could be favored because the proton donor was in short supply on Cu-NS without modification of the proton sponge. However, the *n*-propanol production pathway, in demand for more proton introduction, is adaptively regulated and enhanced accordingly by the Cu-NS with modification of proton sponge.

The $FE_{n\text{-propanol}}$ of the CORR on a catalyst with higher amount of proton sponge and CO pressure (Cu-NS-30% PS under 5 bar CO pressure) was further investigated. Cu-NS-30% PS exhibited $FE_{n\text{-propanol}}$ of 30.6% at −0.49 V *vs.* RHE under 5 bar CO, which was lower than that of Cu-NS-20% PS under 3 bar CO

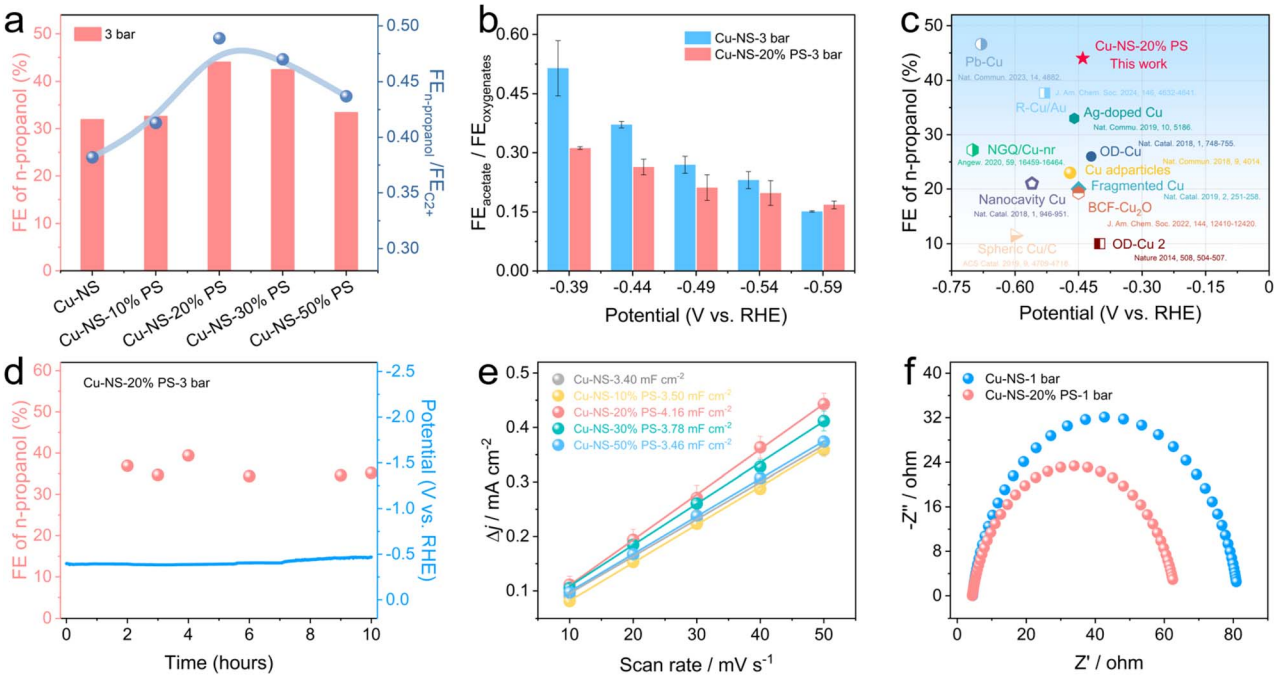

Fig. 4 Electrochemical CORR performance of Cu-NS-*x*% PS ($x = 0$, 10, 20, 30 and 50) under ambient and high CO pressures. (a) $FE_{n\text{-propanol}}$ and $FE_{n\text{-propanol}}/FE_{C_{2+}}$ ratios on Cu-NS-*x*% PS ($x = 0$, 10, 20, 30 and 50) under 3 bar CO. (b) The comparison of $FE_{acetate}/FE_{oxygenates}$ ratios on Cu-NS and Cu-NS-20% PS under 3 bar CO pressure. (c) $FE_{n\text{-propanol}}$ *vs.* potentials for various Cu-based catalysts in the CORR. (d) The chronopotentiometric potential time curve for Cu-NS-20% PS under 3 bar CO at −12 mA cm^{-2} along with the corresponding $FE_{n\text{-propanol}}$. (e) The charging current density differences against scan rates with Cu-NS-*x*% PS ($x = 0$, 10, 20, 30 and 50) as catalysts. (f) Nyquist plots for Cu-NS and Cu-NS-20% PS electrodes in CO-staurated 1 M KOH electrolyte under 1 bar CO.

pressure and higher than that of Cu-NS under 1 bar CO pressure (Fig. 3b and S23†). These results revealed that an excess amount of proton sponge could cover the active sites of the Cu-based catalyst and further suppress the *n*-propanol production. Besides, the CORR performance of Cu-NS-20% PS using different concentrations of KOH (0.5 M and 2 M) as the electrolyte was also scrutinized under 3 bar CO (Fig. S24†). The $FE_{n\text{-propanol}}$ and FE_{C2+} of Cu-NS-20% PS using 1 M KOH as the electrolyte were higher than those of the same catalyst using 0.5 M or 2 M KOH as the electrolyte under 3 bar CO pressure (Fig. S25†). This observation suggests that in higher concentrated alkaline media (*e.g.*, 2 M KOH), the limited proton availability may suppress CO reduction, thereby diminishing C_{2+} product selectivity. Compared with the two catalysts from commercial CuO and proton sponge modified commercial CuO, the as-prepared Cu-NS and Cu-NS-20% PS exhibited higher activity and selectivity towards *n*-propanol during the CORR, which could be attributed to the more abundant active sites in the nanosheet CuO precursor (Fig. S1 and S26†). In order to investigate the CORR performance of CuO-based catalysts from different proton sponge modification methods, CuO-NS was first *in situ* reduced at −0.44 V *vs.* RHE for 30 min, then 20% proton sponge was added to the surface of the Cu-NS to form the Cu-NS-after 20% PS catalyst. As displayed in the results in Fig. 3b and S27,† the $FE_{n\text{-propanol}}$ from Cu-NS-after 20% PS was lower than that from Cu-NS-20% PS at different tested potentials.

Moreover, we directly compared the catalytic performance of Cu-NS-20% PS for *n*-propanol production with that of the reported catalysts (Fig. 4c and Table S1†). It was clearly demonstrated that Cu-NS-20% PS possessed one of the highest $FE_{n\text{-propanol}}$ values to date, and revealed one of the lowest potentials amongst results reported thus far. And the partial current density for *n*-propanol was also greatly improved compared with the bare Cu-NS catalyst under ambient CO pressure, exhibiting pretty good results in H-type cells (Fig. 3c and S28†).

The stability of Cu-NS-20% PS was also evaluated *via* a long-term chronopotentiometry testing. It was found that there was no apparent decay of activity within 10 h operation time (Fig. 4d). Furthermore, the PXRD, XPS, SEM and TEM data of the electrode after the CORR under 3 bar CO test were collected. The characteristic peaks of Cu_2O and Cu observed obviously from the PXRD patterns were found to be similar to the original Cu-NS-20% PS (Fig. 2c and S29†). XPS spectra of the Cu-NS-20% PS after the CORR also exhibited the presence of Cu^+ peaks (Fig. S30†). Besides, the SEM and TEM images showed that the sample still retained the nanosheet morphology (Fig. S31†).

Based on the results and analysis above, the selectivity and activity of *n*-propanol were raised distinctly by rationally introducing a certain amount of proton sponge and appropriate CO pressure. This prompted us to investigate the intrinsic reasons for the enhanced CO conversion to *n*-propanol. To verify the importance of the Cu-NS-20% PS structure, we determined the double-layer capacitance (C_{dl}), which was obtained from the

charging current density at −0.026 V *vs.* RHE against the slope of scan rate (Fig. 4e and S32†). The C_{dl} values of Cu-NS-*x*% PS (*x* = 0, 10, 20, 30 and 50) presented a volcanic trend, and Cu-NS-20% PS showed the highest electrochemically active surface area (ECSA) (Fig. S33 and Table S4†). The trend was similar to the relationship between $FE_{n\text{-propanol}}$ and proton sponge amount on Cu-NS, which further indicated that the active sites of the Cu-based catalyst and the activity of the CORR to *n*-propanol could be enhanced with an optimized proton sponge/Cu ratio, while an excess amount of proton sponge would shield the active sites of the Cu-based catalyst indeed. The Nyquist plots were also measured (Fig. 4f and S34†), and the charge-transfer resistance (R_{ct}) of Cu-NS-20% PS was found to be smaller than that of Cu-NS, suggesting that the proton sponge-modified Cu-based catalyst could efficiently promote the charge transport during the electrocatalytical process in contrast to the control Cu-NS.[55]

Mechanism analysis

To gain in-depth insights into the mechanism of proton sponge-modification of Cu-NS and the pressure-driven electrochemical CORR to *n*-propanol, *in situ* ATR-SEIRAS data were further collected on a custom-made high-pressure spectroelectrochemical setup to probe the intermediates associated with CORR reactivity on Cu-NS-20% PS and Cu-NS under CO pressures of 1 bar and 3 bar, respectively (Fig. S35–S37†). A prominent absorption band in the range of 2072–2025 cm^{-1}, attributed to the C=O stretching mode of atop-adsorbed CO (CO_{atop}), was observed on the Cu-NS-20% PS and Cu-NS at potentials from 0.1 to −0.6 V *vs.* RHE under both 1 bar and 3 bar CO (Fig. 5a, b, d and e). The CO_{atop} band red-shifted as the potential decreased from 0.1 to −0.6 V *vs.* RHE, which was ascribed to the Stark shift.[56,57]

Meanwhile, the peak position of the CO_{atop} band could serve as a proxy to compare absolute CO coverages.[58] The wavenumber of the CO_{atop} band was higher under 3 bar than those under 1 bar for both Cu-NS-20% PS and Cu-NS (Fig. 5c), indicating that the absolute CO_{atop} coverage at 3 bar of CO was higher than that under ambient CO pressure at a controlled potential.[58] Besides, the CO_{atop} band areas of Cu-NS-20% PS and Cu-NS were normalized to the maximum value under both 1 bar and 3 bar CO pressures, respectively (Fig. 5f). We speculated that the elevated CO pressure and modification with proton sponge on Cu-NS could enrich the *CO intermediates, and cause moderate impact of rapid CO_{atop} consumption at large overpotentials. On the other hand, the bands in the range of 1839–1763 cm^{-1} can be assigned to the C=O stretching mode of the bridge-adsorbed CO (CO_b). The Cu-NS-20% PS catalyst presented the strongest CO_b peaks during the CORR from 0.1 to −0.6 V *vs.* RHE under 3 bar CO compared with those of control experiments (Fig. 5a, b, d and e), and it was reported that the cooperation of CO_{atop} and CO_b could facilitate C–C coupling.[59]

To further understand how the *H supply affected the C_2 and C_3 products, well-controlled sets of experiments including linear sweep voltammetry tests, kinetic isotopic effect (KIE) of H/D measurements and *H trapping experiments were conducted. Firstly, the intrinsic H_2O dissociation activity of Cu-NS, with and without proton sponge modification, was investigated by comparing the normalized polarization curves of Cu-NS and Cu-NS-20% PS per ECSA in 1 M KOH under an Ar atmosphere (Fig. 5g and S38†). Both the ECSA-normalized current density and geometric current density of Cu-NS-20% PS were higher than those of Cu-NS, demonstrating that modifying Cu-NS with a proton sponge enhanced the dissociation of H_2O,[60] in good agreement with experimental results (Fig. S22†). Besides, we measured the KIE of H/D on the Cu-NS and Cu-NS-20% PS catalysts. The KIE of H/D is defined as the ratio of $FE_{C_2H_4}$ in H_2O and D_2O, a KIE value larger than 1.5 indicates that water activation affects the reaction rate.[61] The Cu-NS catalyst showed large KIE values of 1.53 and 1.85 at 1 bar and 3 bar CO, respectively, indicating that the sluggish kinetics of H_2O dissociation limited the electrocatalytic CORR process.[62] The Cu-NS-20% PS catalyst exhibited lower KIE values of 1.02 and 1.35 at 1 bar and 3 bar CO, respectively, indicating that the Cu-NS catalyst modified with proton sponge could effectively accelerate H_2O dissociation and promote proton transfer at both 1 bar CO and 3 bar CO pressures (Fig. 5h).[63,64] To further investigate whether *H supply of Cu-NS-20% PS tuned the *n*-propanol selectivity, we conducted the *H trapping experiments using *tert*-butanol (*t*-BuOH) as the *H trapping agent.[64,65] The decrease in the ratio of $FE_{n\text{-propanol}}/FE_{C_2^+}$ on Cu-NS-20% PS was much larger than that on Cu-NS when *t*-BuOH was added to the reaction system (Fig. 5i). This result indicates that the generation of *n*-propanol is closely related to the *H supply on the catalyst surface, and a faster *H supply (proton-sufficient supply) could directionally promote the CORR to produce *n*-propanol.[64]

Density functional theory (DFT) calculations

To further rationalize the impact of the proton sponge on the catalyst performance towards the selective and efficient propanol synthesis, DFT simulations related to the impact of the proton sponge on the oxidation state of the Cu-NS and on the key C-chain growth stage were performed. The proton sponge could adsorb on the Cu_2O surface in different configurations, including the one depicted in Fig. 6a. The proton sponge was mainly attracted to the Cu_2O surface *via* carbon copper interactions, as well as weak interactions of hydrogen atoms with the surface. The presence of the proton sponge substantially increased the energy of formation of oxygen vacancy on the Cu_2O surface (Fig. 6b and S39–S41†), as compared with the pristine Cu_2O (111) surface,[66] preventing the removal of oxygen from the reactive surface and thus preserving the oxidation state of the Cu^+, which coexisted with the metallic Cu^0. The hydrophobic nature of the proton sponge heightened the chemical potential of water [66] in the vicinity of the catalyst surface, therefore, making its formation unfavorable. That also contributed to the coexistence of Cu^+ and Cu^0 oxidation states. Moreover, its non-polar fragments could serve to attract the non-polar hydrogen molecules. Therefore, Cu^+/Cu^0 became stabilized in the presence of the proton sponge.

Given that only *CO was observed and hydrogen-containing species were not detected in the *in situ* ATR-SEIRAS, we are more inclined to rationally follow the *CO + *CO and *CO + *OCCO

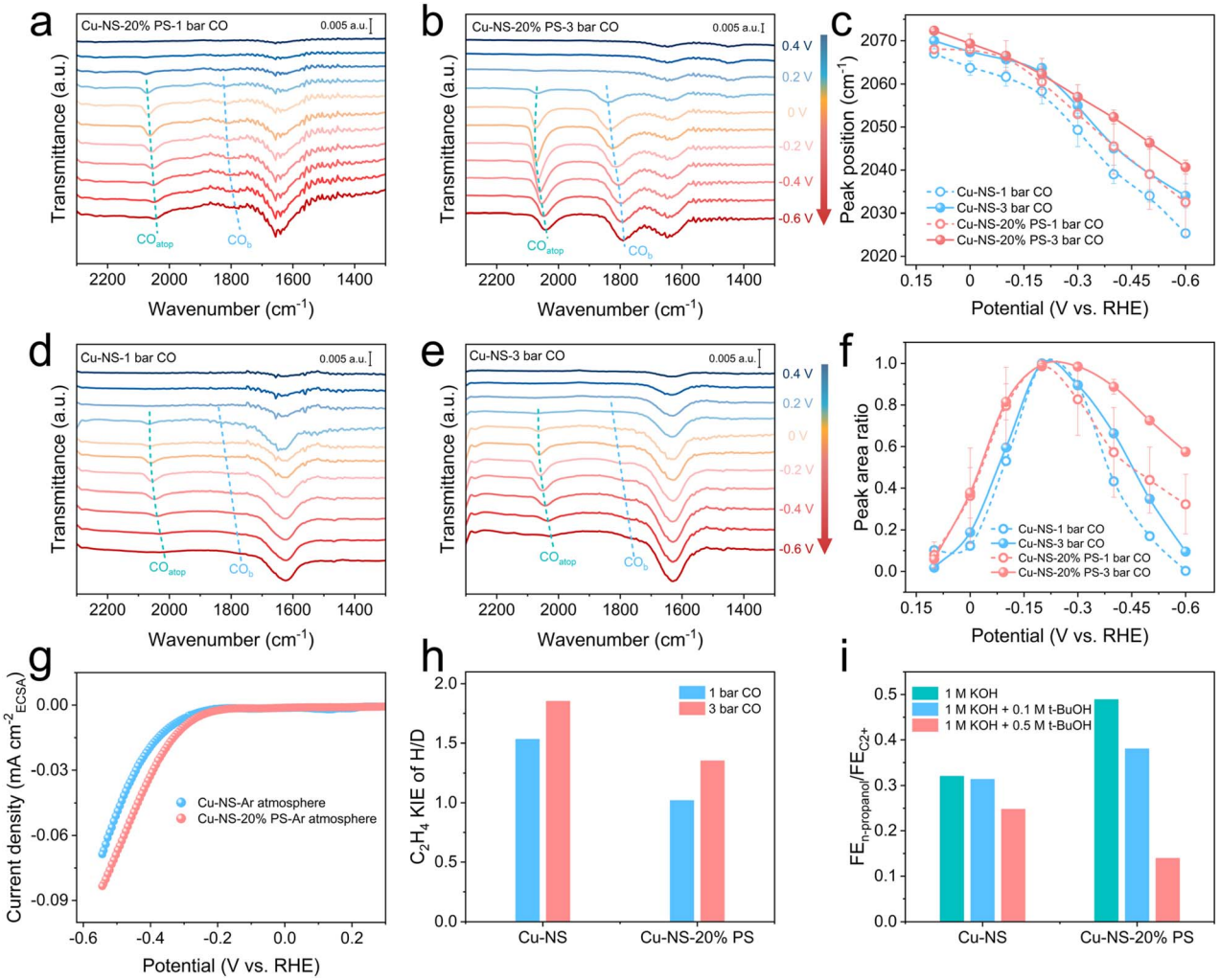

Fig. 5 Mechanism investigation. Potential-dependent SEIRAS investigation of CO_{atop} and CO_b bands on Cu-NS-20% PS under (a) 1 bar CO, (b) 3 bar CO in 0.1 M KOH electrolyte. (c) Potential-dependent SEIRAS investigation of CO_{atop} peak positions on Cu-NS-20% PS and Cu-NS under CO pressures of 1 bar and 3 bar, respectively. Potential-dependent SEIRAS investigation of CO_{atop} and CO_b bands on Cu-NS under (d) 1 bar CO, (e) 3 bar CO in 0.1 M KOH electrolyte. (f) Potential-dependent SEIRAS investigation of CO_{atop} band areas on Cu-NS-20% PS and Cu-NS under pressures of 1 bar and 3 bar CO, respectively. The maximum peak area at each CO pressure was scaled to 1.0. Error bars represent the standard deviation of three independent measurements. (g) The linear sweep voltammetry curve per ECSA in 1 M KOH under an Ar atmosphere for the Cu-NS-20% PS and Cu-NS catalysts, respectively. (h) KIE of H/D in the CORR to C_2H_4 performance on Cu-NS and Cu-NS-20% PS at −0.44 V *vs.* RHE under 1 bar and 3 bar CO, respectively. (i) Ratios of $FE_{n\text{-propanol}}/FE_{C_{2+}}$ on Cu-NS and Cu-NS-20% PS at −0.44 V *vs.* RHE in 1 M KOH solution with the addition of 0 M, 0.1 M and 0.5 M *t*-BuOH under 3 bar CO pressure.

coupling mechanisms to generate *n*-propanol.[28,67] Considering the C-chain growth on the Cu^+/Cu^0 and Cu^0 surfaces, it turned out that the adsorption of *CO, *OCCO and *OCCOCO intermediates on Cu^+/Cu^0 was more favorable than that on the fully reduced (111) surface of fcc-Cu (Fig. 6c and S42–S44†). Indeed, for *OCCOCO, the adsorption energy on Cu^+/Cu^0 was −1.76 eV; while for the metallic Cu system, it was −0.66 eV. In both Cu^+/Cu^0 and Cu^0 systems, *OCCOCO attached to the surface *via* the terminal carbon atoms on both sides interacting with surface copper atoms, while neither the middle carbon atom nor oxygen atoms participated in the adsorption. However, in particular, for the mixed valence Cu^+/Cu^0 system, the distance between copper sites perfectly matched with the length of the C_3 chain of the *OCCOCO intermediates (Fig. S45 and S46†), which was another factor responsible for its enhanced selectivity and activity towards the C_3 product.

On the other hand, the proton sponge can locally stabilize the dissociated water molecules, collecting the H^+ inside. The $[\text{proton sponge–H}]^+$ complex attracts OH^- along with hydration water molecules due to the electrostatic interaction. The system with H^+ in the proton sponge and hydrated OH^- is less energetically favorable by 0.43 eV than the proton sponge–-water system (Fig. S47†). However, the electrochemical overpotential applied to the system during the reaction (−0.44 V *vs.* RHE) is sufficient to overcome this energy barrier, that is, the negatively charged catalyst surface by electrostatic interaction provokes water dissociation; the proton sponge collects the resulting protons and promotes proton supply (Fig. S48†).

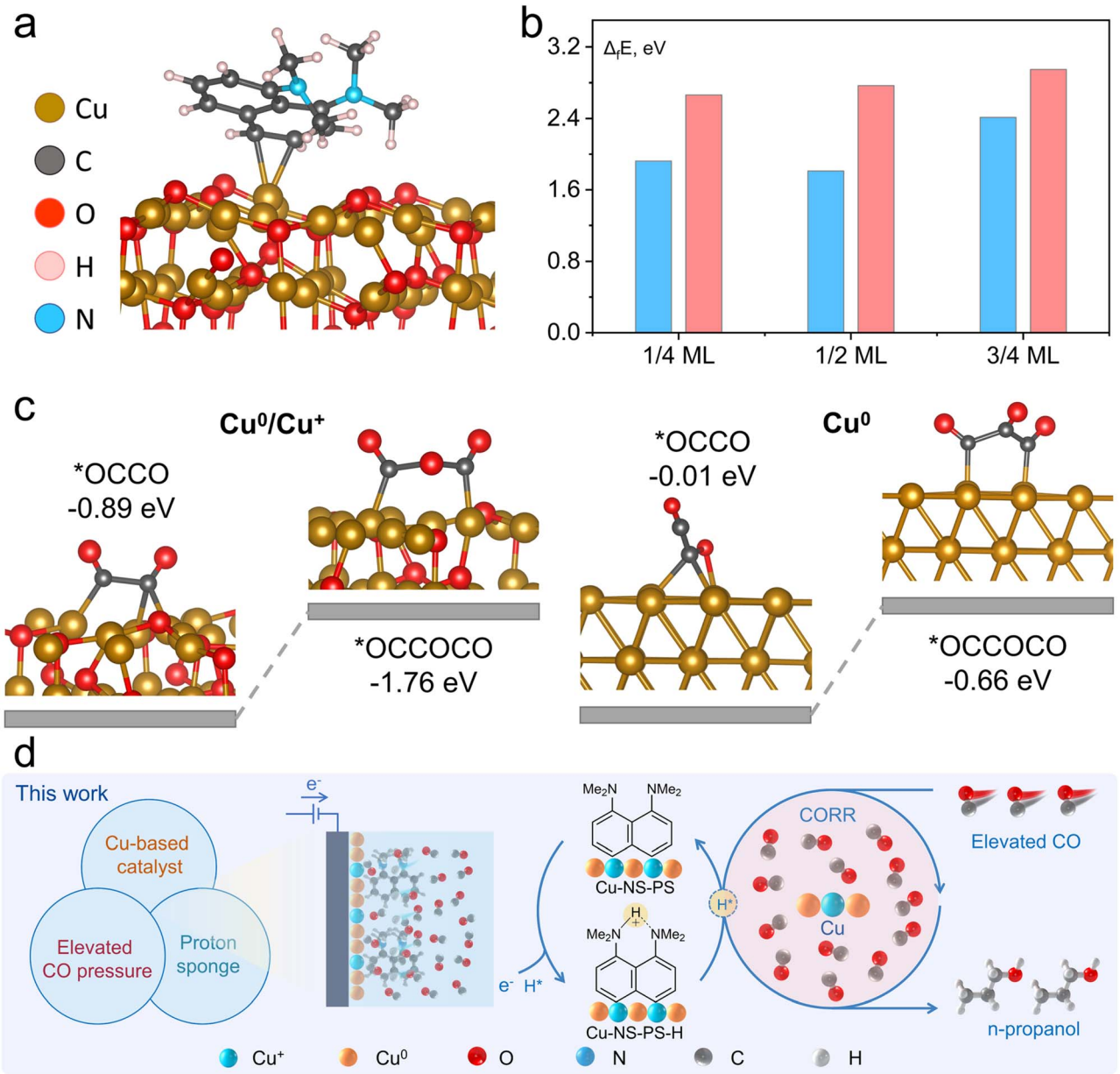

Fig. 6 The impact of the proton sponge on the copper oxidation state on the surface and the adsorption energetics of the key C-chain growth intermediates. (a) Adsorption of the proton sponge molecule on the Cu_2O (111) surface. (b) The formation energies of oxygen vacancies on the pristine Cu_2O (111) surface (blue, from ref. 66) and Cu_2O (111) surface covered with proton sponge (pink). (c) Adsorption intermediates and energies on the Cu^0/Cu^+ (111) Cu_2O surface and Cu (111) surface. (d) Schematic illustration of the cooperative promotion of electroreduction of CO to *n*-propanol on Cu-based catalysts by the proton regulator and elevated pressure.

Based on a series of control experiments and DFT calculations above, it could be observed that both the elevated CO pressure and proton sponge-modification on Cu-based catalysts played indispensable roles in enhancing *CO coverage and *H supply for subsequent *CO + *CO and *CO + *OCCO coupling. Besides, the mixed-valence Cu^+/Cu^0 system exhibits an optimal geometric configuration, where the interatomic spacing between adjacent copper sites aligns precisely with the molecular dimensions of the C_3 backbone in the *OCCOCO intermediate. The synergistic optimization of multiple reaction parameters in proton sponge-functionalized Cu catalysts leads to significantly enhanced *n*-propanol generation efficiency in the CORR (Fig. 6d).

Conclusions

In summary, we present a strategy to significantly improve the selectivity of *n*-propanol in CO electrolysis by cooperation of the binding proton sponge on Cu-NS and the CO pressure regulation. Through conveniently regulating the amount of proton

sponge and CO pressure, we demonstrate a CO to *n*-propanol conversion with an FE of 44.0% ± 2.3% for *n*-propanol on the Cu-NS-20% PS catalyst at −0.44 V *vs.* RHE under 3 bar CO pressure, which is ~1.4-fold higher than that on the pure Cu-NS catalyst under the same CO pressure. The oxygenated products are enhanced accompanied by a decrease of ethylene selectivity by increasing the CO pressure for both pure Cu-NS and Cu-NS-20% PS. Simultaneously, the selectivity of the multiple proton coupled electron transfer product (*n*-propanol) was enhanced effectively on Cu-NS-20% PS compared with the pure Cu-NS. This is due to the appropriate *CO coverage, matched with the suitable *H intermediates, and the perfect distance between copper sites matching the length of the C_3 chain of the *OCCOCO intermediates after modification with proton sponge under elevated CO pressure. Experimental results and *in situ* ATR-SEIRAS demonstrated that sufficient *CO coverage and *H intermediate could be provided by appropriate CO pressure and proton sponge-modification, respectively, for subsequent C_1–C_1 and C_1–C_2 coupling. *In situ* Raman spectra and DFT calculations further revealed that Cu^+ species existed stably in the proton sponge-modified Cu-based catalyst, leading to a low energy barrier in the potential-determining C_1–C_1 and C_1–C_2 coupling steps.

Data availability

The data supporting this article have been included as part of the ESI.†

Author contributions

L. P., S. Y., J. L. and B. H. supervised the project. R. Q. designed the high-pressure *in situ* Raman cell setup and *in situ* ATR-SEIRAS cell setup. R. Q. and B. Z. synthesized the catalysts. R. Q., L. C., J. L., C. L. and J. Z. carried out electrochemical experiments. R. Q., L. C., L. D. and Y. D. characterized the materials. O. A. S. and M. A. S. carried out DFT calculations. R. Q., N. F. and J. Y. conducted the *in situ* ATR-SEIRAS experiment. R. Q., Y. J., J.-C. D. and J.-F. L. conducted the *in situ* Raman spectroscopy experiment. T. X., I. A. and J. Z. contributed to data analysis. R. Q., J. L., L. P., J. L., S. Y. and B. H. co-wrote the manuscript. All authors discussed the results and contributed to the preparation of the manuscript.

Conflicts of interest

The authors declare no conflict of interest.

Acknowledgements

L. P. acknowledges funding support from the National Natural Science Foundation of China (grant no. 22373080) and Fujian Provincial Natural Science Foundation of China (grant no. 2024J08008). J. L. acknowledges funding support from the National Natural Science Foundation of China (grant no. 22078274). S. Y. acknowledges funding support from the Natural Science Foundation of Fujian Province of China (no. 2022J05009), the Fundamental Research Funds for the Central Universities (grant no. 20720240054), the Nan-qiang Youth Scholar Program of Xiamen University and Xiaomi Young Talents Program/Xiaomi Foundation.

Notes and references

1 S. Nitopi, E. Bertheussen, S. B. Scott, X. Liu, A. K. Engstfeld, S. Horch, B. Seger, I. E. L. Stephens, K. Chan, C. Hahn, J. K. Norskov, T. F. Jaramillo and I. Chorkendorff, Progress and perspectives of electrochemical CO_2 reduction on copper in aqueous electrolyte, *Chem. Rev.*, 2019, **119**, 7610–7672.

2 S. Jin, Z. Hao, K. Zhang, Z. Yan and J. Chen, Advances and challenges for the electrochemical reduction of CO_2 to CO: from fundamentals to industrialization, *Angew. Chem., Int. Ed.*, 2021, **60**, 20627–20648.

3 J. D. Yi, X. Gao, H. Zhou, W. Chen and Y. Wu, Design of Co-Cu diatomic site catalysts for high-efficiency synergistic CO_2 electroreduction at industrial-level current density, *Angew. Chem., Int. Ed.*, 2022, **61**, e202212329.

4 H. S. Jeon, J. Timoshenko, F. Scholten, I. Sinev, A. Herzog, F. T. Haase and B. Roldan Cuenya, Operando insight into the correlation between the structure and composition of CuZn nanoparticles and their selectivity for the electrochemical CO_2 reduction, *J. Am. Chem. Soc.*, 2019, **141**, 19879–19887.

5 Y. R. Wang, M. Liu, G. K. Gao, Y. L. Yang, R. X. Yang, H. M. Ding, Y. Chen, S. L. Li and Y. Q. Lan, Implanting numerous hydrogen-bonding networks in a Cu-porphyrin-based nanosheet to boost CH_4 selectivity in neutral-media CO_2 electroreduction, *Angew. Chem., Int. Ed.*, 2021, **60**, 21952–21958.

6 L. Xiong, X. Zhang, L. Chen, Z. Deng, S. Han, Y. Chen, J. Zhong, H. Sun, Y. Lian, B. Yang, X. Yuan, H. Yu, Y. Liu, X. Yang, J. Guo, M. H. Rummeli, Y. Jiao and Y. Peng, Geometric modulation of local CO flux in Ag@Cu_2O nanoreactors for steering the CO_2RR pathway toward high-efficacy methane production, *Adv. Mater.*, 2021, **33**, e2101741.

7 T. Zheng, C. Liu, C. Guo, M. Zhang, X. Li, Q. Jiang, W. Xue, H. Li, A. Li, C.-W. Pao, J. Xiao, C. Xia and J. Zeng, Copper-catalysed exclusive CO_2 to pure formic acid conversion *via* single-atom alloying, *Nat. Nanotech.*, 2021, **16**, 1386–1393.

8 H. Yang, Y. Wu, G. Li, Q. Lin, Q. Hu, Q. Zhang, J. Liu and C. He, Scalable production of efficient single-atom copper decorated carbon membranes for CO_2 electroreduction to methanol, *J. Am. Chem. Soc.*, 2019, **141**, 12717–12723.

9 J. Liu, D. Yang, Y. Zhou, G. Zhang, G. Xing, Y. Liu, Y. Ma, O. Terasaki, S. Yang and L. Chen, Tricycloquinazoline-based 2D conductive metal-organic frameworks as promising electrocatalysts for CO_2 reduction, *Angew. Chem., Int. Ed.*, 2021, **60**, 14473–14479.

10 W. Li, Z. Yin, Z. Gao, G. Wang, Z. Li, F. Wei, X. Wei, H. Peng, X. Hu, L. Xiao, J. Lu and L. Zhuang, Bifunctional ionomers for efficient co-electrolysis of CO_2 and pure water towards

ethylene production at industrial-scale current densities, *Nat. Energy*, 2022, **7**, 835–843.

11 X. Chen, J. Chen, N. M. Alghoraibi, D. A. Henckel, R. Zhang, U. O. Nwabara, K. E. Madsen, P. J. A. Kenis, S. C. Zimmerman and A. A. Gewirth, Electrochemical CO_2-to-ethylene conversion on polyamine-incorporated Cu electrodes, *Nat. Catal.*, 2020, **4**, 20–27.

12 Y. Zhang, P. Li, C. Zhao, G. Zhou, F. Zhou, Q. Zhang, C. Su and Y. Wu, Multicarbons generation factory: CuO/Ni single atoms tandem catalyst for boosting the productivity of CO_2 electrocatalysis, *Sci. Bull.*, 2022, **67**, 1679–1687.

13 L. Ding, N. Zhu, Y. Hu, Z. Chen, P. Song, T. Sheng, Z. Wu and Y. Xiong, Over 70% faradaic efficiency for CO_2 electroreduction to ethanol enabled by potassium dopant-tuned interaction between copper sites and intermediates, *Angew. Chem., Int. Ed.*, 2022, **61**, e202209268.

14 C. Chen, X. Yan, S. Liu, Y. Wu, Q. Wan, X. Sun, Q. Zhu, H. Liu, J. Ma, L. Zheng, H. Wu and B. Han, Highly efficient electroreduction of CO_2 to C_{2+} alcohols on heterogeneous dual active sites, *Angew. Chem., Int. Ed.*, 2020, **59**, 16459–16464.

15 B. Yang, L. Chen, S. Xue, H. Sun, K. Feng, Y. Chen, X. Zhang, L. Xiao, Y. Qin, J. Zhong, Z. Deng, Y. Jiao and Y. Peng, Electrocatalytic CO_2 reduction to alcohols by modulating the molecular geometry and Cu coordination in bicentric copper complexes, *Nat. Commun.*, 2022, **13**, 5122.

16 X. F. Qiu, J. R. Huang, C. Yu, Z. H. Zhao, H. L. Zhu, Z. Ke, P. Q. Liao and X. M. Chen, A stable and conductive covalent organic framework with isolated active sites for highly selective electroreduction of carbon dioxide to acetate, *Angew. Chem., Int. Ed.*, 2022, **61**, e202206470.

17 C. Peng, G. Luo, J. Zhang, M. Chen, Z. Wang, T. K. Sham, L. Zhang, Y. Li and G. Zheng, Double sulfur vacancies by lithium tuning enhance CO_2 electroreduction to n-propanol, *Nat. Commun.*, 2021, **12**, 1580.

18 C. Long, X. Liu, K. Wan, Y. Jiang, P. An, C. Yang, G. Wu, W. Wang, J. Guo, L. Li, K. Pang, Q. Li, C. Cui, S. Liu, T. Tan and Z. Tang, Regulating reconstruction of oxide-derived Cu for electrochemical CO_2 reduction toward n-propanol, *Sci. Adv.*, 2023, **9**, eadi6119.

19 S. Lee, D. Kim and J. Lee, Electrocatalytic production of C_3–C_4 compounds by conversion of CO_2 on a chloride-induced Bi-phasic Cu_2O-Cu catalyst, *Angew. Chem., Int. Ed.*, 2015, **54**, 14701–14705.

20 M. Jouny, W. Luc and F. Jiao, High-rate electroreduction of carbon monoxide to multi-carbon products, *Nat. Catal.*, 2018, **1**, 748–755.

21 M. Fang, L. Xu, H. Zhang, Y. Zhu and W. Y. Wong, Metalloporphyrin-linked mercurated graphynes for ultrastable CO_2 electroreduction to CO with nearly 100% selectivity at a current density of 1.2 A cm^{-2}, *J. Am. Chem. Soc.*, 2022, **144**, 15143–15154.

22 W. Ma, X. He, W. Wang, S. Xie, Q. Zhang and Y. Wang, Electrocatalytic reduction of CO_2 and CO to multi-carbon compounds over Cu-based catalysts, *Chem. Soc. Rev.*, 2021, **50**, 12897–12914.

23 C. Zhao, G. Luo, X. Liu, W. Zhang, Z. Li, Q. Xu, Q. Zhang, H. Wang, D. Li, F. Zhou, Y. Qu, X. Han, Z. Zhu, G. Wu, J. Wang, J. Zhu, T. Yao, Y. Li, H. J. M. Bouwmeester and Y. Wu, In situ topotactic transformation of an interstitial alloy for CO electroreduction, *Adv. Mater.*, 2020, **32**, e2002382.

24 G. Wu, Y. Song, Q. Zheng, C. Long, T. Fan, Z. Yang, X. Huang, Q. Li, Y. Sun, L. Zuo, S. Lei and Z. Tang, Selective electroreduction of CO_2 to n-propanol in two-step tandem catalytic system, *Adv. Energy Mater.*, 2022, **12**, 2202054.

25 T.-T. Zhuang, Y. Pang, Z.-Q. Liang, Z. Wang, Y. Li, C.-S. Tan, J. Li, C. T. Dinh, P. De Luna, P.-L. Hsieh, T. Burdyny, H.-H. Li, M. Liu, Y. Wang, F. Li, A. Proppe, A. Johnston, D.-H. Nam, Z.-Y. Wu, Y.-R. Zheng, A. H. Ip, H. Tan, L.-J. Chen, S.-H. Yu, S. O. Kelley, D. Sinton and E. H. Sargent, Copper nanocavities confine intermediates for efficient electrosynthesis of C_3 alcohol fuels from carbon monoxide, *Nat. Catal.*, 2018, **1**, 946–951.

26 J. Liu, F. You, B. He, Y. Wu, D. Wang, W. Zhou, C. Qian, G. Yang, G. Liu, H. Wang, Y. Guo, L. Gu, L. Feng, S. Li and Y. Zhao, Directing the architecture of surface-clean Cu_2O for CO electroreduction, *J. Am. Chem. Soc.*, 2022, **144**, 12410–12420.

27 L. Fan, Q. Geng, L. Ma, C. Wang, J.-X. Li, W. Zhu, R. Shao, W. Li, X. Feng, Y. Yamauchi, C. Li and L. Jiang, Evoking C_{2+} production from electrochemical CO_2 reduction by the steric confinement effect of ordered porous Cu_2O, *Chem. Sci.*, 2023, **14**, 13851–13859.

28 X. Wang, P. Ou, A. Ozden, S.-F. Hung, J. Tam, C. M. Gabardo, J. Y. Howe, J. Sisler, K. Bertens, F. P. García de Arquer, R. K. Miao, C. P. O'Brien, Z. Wang, J. Abed, A. S. Rasouli, M. Sun, A. H. Ip, D. Sinton and E. H. Sargent, Efficient electrosynthesis of n-propanol from carbon monoxide using a Ag-Ru-Cu catalyst, *Nat. Energy*, 2022, **7**, 170–176.

29 W. Niu, Z. Chen, W. Guo, W. Mao, Y. Liu, Y. Guo, J. Chen, R. Huang, L. Kang, Y. Ma, Q. Yan, J. Ye, C. Cui, L. Zhang, P. Wang, X. Xu and B. Zhang, Pb-rich Cu grain boundary sites for selective CO-to-n-propanol electroconversion, *Nat. Commun.*, 2023, **14**, 4882.

30 H. Phong Duong, J. G. Rivera de la Cruz, N. H. Tran, J. Louis, S. Zanna, D. Portehault, A. Zitolo, M. Walls, D. V. Peron, M. W. Schreiber, N. Menguy and M. Fontecave, Silver and copper nitride cooperate for CO electroreduction to propanol, *Angew. Chem., Int. Ed.*, 2023, **62**, e20231078.

31 X. Wang, Z. Wang, T. T. Zhuang, C. T. Dinh, J. Li, D. H. Nam, F. Li, C. W. Huang, C. S. Tan, Z. Chen, M. Chi, C. M. Gabardo, A. Seifitokaldani, P. Todorovic, A. Proppe, Y. Pang, A. R. Kirmani, Y. Wang, A. H. Ip, L. J. Richter, B. Scheffel, A. Xu, S. C. Lo, S. O. Kelley, D. Sinton and E. H. Sargent, Efficient upgrading of CO to C_3 fuel using asymmetric C-C coupling active sites, *Nat. Commun.*, 2019, **10**, 5186.

32 Y. Pang, J. Li, Z. Wang, C.-S. Tan, P.-L. Hsieh, T.-T. Zhuang, Z.-Q. Liang, C. Zou, X. Wang, P. De Luna, J. P. Edwards, Y. Xu, F. Li, C.-T. Dinh, M. Zhong, Y. Lou, D. Wu, L.-J. Chen, E. H. Sargent and D. Sinton, Efficient electrocatalytic conversion of carbon monoxide to

propanol using fragmented copper, *Nat. Catal.*, 2019, **2**, 251–258.

33 J. Li, F. Che, Y. Pang, C. Zou, J. Y. Howe, T. Burdyny, J. P. Edwards, Y. Wang, F. Li, Z. Wang, P. De Luna, C. T. Dinh, T. T. Zhuang, M. I. Saidaminov, S. Cheng, T. Wu, Y. Z. Finfrock, L. Ma, S. H. Hsieh, Y. S. Liu, G. A. Botton, W. F. Pong, X. Du, J. Guo, T. K. Sham, E. H. Sargent and D. Sinton, Copper adparticle enabled selective electrosynthesis of n-propanol, *Nat. Commun.*, 2018, **9**, 4614.

34 Z. Gu, H. Shen, Z. Chen, Y. Yang, C. Yang, Y. Ji, Y. Wang, C. Zhu, J. Liu, J. Li, T.-K. Sham, X. Xu and G. Zheng, Efficient electrocatalytic CO_2 reduction to C_{2+} alcohols at defect-site-rich Cu surface, *Joule*, 2021, **5**, 429–440.

35 J. Li, Z. Wang, C. McCallum, Y. Xu, F. Li, Y. Wang, C. M. Gabardo, C.-T. Dinh, T.-T. Zhuang, L. Wang, J. Y. Howe, Y. Ren, E. H. Sargent and D. Sinton, Constraining CO coverage on copper promotes high-efficiency ethylene electroproduction, *Nat. Catal.*, 2019, **2**, 1124–1131.

36 R. Qiu, J. Li, L. Cui, S. Yang, L. Peng and J. Li, Recent advances in selective electrochemical reduction of CO_2/CO at elevated pressures, *Sci. Sin. Chim.*, 2023, **53**, 1405–1418.

37 S. J. Raaijman, M. P. Schellekens, P. J. Corbett and M. T. M. Koper, High-pressure CO electroreduction at silver produces ethanol and propanol, *Angew. Chem., Int. Ed.*, 2021, **60**, 21732–21736.

38 R. Qiu, J. Jia, L. Peng, R. Li, S. Yan, J. Li, J. Zhang, D. T. Sun, Z. Lan, T. Xue, G. Xu, L. Cui, Z. Lv, C. Li, Y. Hong, Y. Guo, B. Ren, S. Yang, J. Li and B. Han, Enhanced electroreduction of CO_2 to ethanol *via* enriched intermediates at high CO_2 pressures, *Green Chem.*, 2023, **25**, 684–691.

39 S. Dey, F. Masero, E. Brack, M. Fontecave and V. Mougel, Electrocatalytic metal hydride generation using CPET mediators, *Nature*, 2022, **607**, 499–506.

40 P. Garrido-Barros, J. Derosa, M. J. Chalkley and J. C. Peters, Tandem electrocatalytic N_2 fixation *via* proton-coupled electron transfer, *Nature*, 2022, **609**, 71–76.

41 L. Fan, C.-Y. Liu, P. Zhu, C. Xia, X. Zhang, Z.-Y. Wu, Y. Lu, T. P. Senftle and H. Wang, Proton sponge promotion of electrochemical CO_2 reduction to multi-carbon products, *Joule*, 2022, **6**, 205–220.

42 T. Ishikawa, *Superbases for Organic Synthesis: Guanidines, Amidines and Phosphazenes and Related Organocatalysts*, Wiley, 2009.

43 R. W. Alder, P. S. Bowman, W. R. S. Steele and D. R. Winterm, The remarkable basicity of 1,8-bis(dirnethylamino) naphthalene, *Chem. Commun.*, 1968, 723–724.

44 N. G. Korzhenevskaya, G. Schroeder, B. Brzezinski and V. I. Rybachenko, Concept of superbasicity of 1,8-bis(dialkylamino)naphthalenes, *Russ. J. Org. Chem.*, 2001, **37**, 1603–1610.

45 Y. Deng, A. D. Handoko, Y. Du, S. Xi and B. S. Yeo, In situ Raman spectroscopy of copper and copper oxide surfaces during electrochemical oxygen evolution reaction: identification of Cu^{III} oxides as catalytically active species, *ACS Catal.*, 2016, **6**, 2473–2481.

46 W. Liu, P. Zhai, A. Li, B. Wei, K. Si, Y. Wei, X. Wang, G. Zhu, Q. Chen, X. Gu, R. Zhang, W. Zhou and Y. Gong, Electrochemical CO_2 reduction to ethylene by ultrathin CuO nanoplate arrays, *Nat. Commun.*, 2022, **13**, 1877.

47 Z. Z. Wu, X. L. Zhang, Z. Z. Niu, F. Y. Gao, P. P. Yang, L. P. Chi, L. Shi, W. S. Wei, R. Liu, Z. Chen, S. Hu, X. Zheng and M. R. Gao, Identification of Cu(100)/Cu(111) interfaces as superior active sites for CO dimerization during CO_2 electroreduction, *J. Am. Chem. Soc.*, 2022, **144**, 259–269.

48 G. Zhang, Z. J. Zhao, D. Cheng, H. Li, J. Yu, Q. Wang, H. Gao, J. Guo, H. Wang, G. A. Ozin, T. Wang and J. Gong, Efficient CO_2 electroreduction on facet-selective copper films with high conversion rate, *Nat. Commun.*, 2021, **12**, 5745.

49 M. Wu, D. Huang, F. Lai, R. Yang, Y. Liu, J. Fang, T. Zhai and Y. Liu, Sequential *CO management *via* controlling *in situ* reconstruction for efficient industrial-current-density CO_2-to-C_{2+} electroreduction, *Proc. Natl. Acad. Sci. U.S.A.*, 2023, **120**, e2302851120.

50 Y. Zhao, X.-G. Zhang, N. Bodappa, W.-M. Yang, Q. Liang, P. M. Radjenovica, Y.-H. Wang, Y.-J. Zhang, J.-C. Dong, Z.-Q. Tian and J.-F. Li, Elucidating electrochemical CO_2 reduction reaction processes on Cu(hkl) single-crystal surfaces by *in situ* Raman spectroscopy, *Energy Environ. Sci.*, 2022, **15**, 3968–3977.

51 Y. Zhao, X. Chang, A. S. Malkani, X. Yang, L. Thompson, F. Jiao and B. Xu, Speciation of Cu surfaces during the electrochemical CO reduction reaction, *J. Am. Chem. Soc.*, 2020, **142**, 9735–9743.

52 B. Zhao, F. Chen, C. Cheng, L. Li, C. Liu and B. Zhang, C_{60}-stabilized Cu^+ sites boost electrocatalytic reduction of CO_2 to C_{2+} products, *Adv. Energy Mater.*, 2023, **13**, 2204346.

53 H. J. Peng, M. T. Tang, J. Halldin Stenlid, X. Liu and F. Abild-Pedersen, Trends in oxygenate/hydrocarbon selectivity for electrochemical CO_2 reduction to C_2 products, *Nat. Commun.*, 2022, **13**, 1399.

54 C. W. Li, J. Ciston and M. W. Kanan, Electroreduction of carbon monoxide to liquid fuel on oxide-derived nanocrystalline copper, *Nature*, 2014, **508**, 504–507.

55 S. Jia, Q. Zhu, M. Chu, S. Han, R. Feng, J. Zhai, W. Xia, M. He, H. Wu and B. Han, Hierarchical metal-polymer hybrids for enhanced CO_2 electroreduction, *Angew. Chem., Int. Ed.*, 2021, **60**, 10977–10982.

56 S. Zhu, B. Jiang, W. B. Cai and M. Shao, Direct observation on reaction intermediates and the role of bicarbonate anions in CO_2 electrochemical reduction reaction on Cu surfaces, *J. Am. Chem. Soc.*, 2017, **139**, 15664–15667.

57 Y. Kim, S. Park, S.-J. Shin, W. Choi, B. K. Min, H. Kim, W. Kim and Y. J. Hwang, Time-resolved observation of C–C coupling intermediates on Cu electrodes for selective electrochemical CO_2 reduction, *Energy Environ. Sci.*, 2020, **13**, 4301–4311.

58 J. Hou, X. Chang, J. Li, B. Xu and Q. Lu, Correlating CO coverage and CO electroreduction on Cu *via* high-pressure

in situ spectroscopic and reactivity investigations, *J. Am. Chem. Soc.*, 2022, **144**, 22202–22211.

59 T. C. Chou, C. C. Chang, H. L. Yu, W. Y. Yu, C. L. Dong, J. J. Velasco-Velez, C. H. Chuang, L. C. Chen, J. F. Lee, J. M. Chen and H. L. Wu, Controlling the oxidation state of the Cu electrode and reaction intermediates for electrochemical CO_2 reduction to ethylene, *J. Am. Chem. Soc.*, 2020, **142**, 2857–2867.

60 K. Sun, X. Wu, Z. Zhuang, L. Liu, J. Fang, L. Zeng, J. Ma, S. Liu, J. Li, R. Dai, X. Tan, K. Yu, D. Liu, W. C. Cheong, A. Huang, Y. Liu, Y. Pan, H. Xiao and C. Chen, Interfacial water engineering boosts neutral water reduction, *Nat. Commun.*, 2022, **13**, 6260.

61 W. Li, F. Li, H. Yang, X. Wu, P. Zhang, Y. Shan and L. Sun, A bio-inspired coordination polymer as outstanding water oxidation catalyst *via* second coordination sphere engineering, *Nat. Commun.*, 2019, **10**, 5074.

62 S. Chen, X. Li, C. W. Kao, T. Luo, K. Chen, J. Fu, C. Ma, H. Li, M. Li, T. S. Chan and M. Liu, Unveiling the proton-feeding effect in sulfur-doped Fe-N-C single-atom catalyst for enhanced CO_2 electroreduction, *Angew. Chem., Int. Ed.*, 2022, **61**, e202206233.

63 W. Ma, S. Xie, T. Liu, Q. Fan, J. Ye, F. Sun, Z. Jiang, Q. Zhang, J. Cheng and Y. Wang, Electrocatalytic reduction of CO_2 to ethylene and ethanol through hydrogen-assisted C–C coupling over fluorine-modified copper, *Nat. Catal.*, 2020, **3**, 478–487.

64 T. Zhang, B. Yuan, W. Wang, J. He and X. Xiang, Tailoring *H intermediate coverage on the $CuAl_2O_4$/CuO catalyst for enhanced electrocatalytic CO_2 reduction to ethanol, *Angew. Chem., Int. Ed.*, 2023, **62**, e202302096.

65 C. Choi, S. Kwon, Y. Gao, S. Cheon, J. Li, F. Menges, W. A. Goddard 3rd and H. Wang, CO_2-promoted electrocatalytic reduction of chlorinated hydrocarbons, *J. Am. Chem. Soc.*, 2024, **146**, 8486–8491.

66 G. Ma, O. A. Syzgantseva, Y. Huang, D. Stoian, J. Zhang, S. Yang, W. Luo, M. Jiang, S. Li, C. Chen, M. A. Syzgantseva, S. Yan, N. Chen, L. Peng, J. Li and B. Han, A hydrophobic Cu/Cu_2O sheet catalyst for selective electroreduction of CO to ethanol, *Nat. Commun.*, 2023, **14**, 501.

67 C. Long, K. Wan, Y. Chen, L. Li, Y. Jiang, C. Yang, Q. Wu, G. Wu, P. Xu, J. Li, X. Shi, Z. Tang and C. Cui, Steering the reconstruction of oxide-derived Cu by secondary metal for electrosynthesis of n-propanol from CO, *J. Am. Chem. Soc.*, 2024, **146**, 4632–4641.